Periodically Driven Nonlinear Reid Oscillators

Konstantinos Kaloudis
(joint work with Tassos Bountis and Christos Spitas)

Department of Mechanical and Aerospace Engineering
Nazarbayev University

VI Dynamics Days Central Asia
Nur–Sultan, Kazakhstan, 02-05/06/2020

NAZARBAYEV UNIVERSITY

Outline

1. Nonlinear extensions of hysteretic damping models
2. SDOF Bishop model
3. SDOF Reid model
4. Arrays of coupled nonlinear Reid oscillators
5. Conclusions & Future Research

Nonlinear extensions of hysteretic damping models

Bishop's model I

- Hysteretic damping: energy loss per cycle to be independent of the deformation frequency.
- Applications: seismic behavior, composite beam modeling, rotor dynamics and material modeling.

Bishop's model

$$M\ddot{x} + \frac{h}{\omega}\dot{x} + kx = F\exp\{i\omega t\}, \tag{1}$$

where x denotes the particle displacement from equilibrium. With $x = R\exp\{i\omega t\}$, we may write $h\dot{x}/\omega \to ihx$, and end up with the equation

$$M\ddot{x} + (k + ih)\,x = F\exp\{i\omega t\}. \tag{2}$$

Bishop's model II

$$M\ddot{x} + (k + ih)\,x = M\ddot{x} + k\,(1 + i\mu)\,x = F\exp\{i\omega t\}. \qquad (3)$$

- Complex ODE: Analytical solutions for N–DOF case.
- For a spring-and-damper system, we have a (complex restoring) force $f = (k + ih)x = k(1 + i\mu)x$, with $\mu = h/k$, thus allowing for the desired frequency independent response.
- $h << k \rightarrow$ viscous damping approximation.

Drawbacks: Numerical instabilities, non–causality (force anticipates the deformation history).
⋄ Frequency domain representation, time domain (Hilbert transform).

Reid's model I

Reid's model

$$M\ddot{x} + c\left|\frac{x}{\dot{x}}\right|\dot{x} + kx = M\ddot{x} + kx\left(1 + \frac{c}{k}\mathrm{sgn}(x\dot{x})\right) = F\sin\omega t, \qquad (4)$$

where $\mathrm{sgn}(\cdot)$ is the sign function, x denotes the particle displacement from equilibrium, c is the damping coefficient, and k quantifies the (linear) stiffness.

- "Quasi–linear" real differential equation → solutions are directly physically interpretable.
- The oscillator is frequency independent and yields work per cycle that is proportional the squared amplitude.
- Drawbacks: discontinuity at the points of stress–strain reversal, non–physical hysteretic loops.
- Various modifications of the model have been proposed to make it more realistic.

Nonlinear extensions

- Effect of adding a nonlinear stiffness term to our models to explore its influence on the dynamics.
- Realistic springs are in general not linear, and may include nonlinearities that depend on the displacement.
- Symmetric springs, where the lowest order nonlinearities are cubic in the displacement.

$$M\ddot{x} + \omega_1^2\,(1 + i\mu)\,x + \epsilon\,x^3 = F\exp\{i\omega t\}. \text{ (Bishop)} \tag{5}$$

$$M\ddot{x} + c\left|\frac{x}{\dot{x}}\right|\dot{x} + kx + \epsilon x^3 = f\sin\omega t. \text{ (Reid)} \tag{6}$$

SDOF Bishop model

Periodic solutions

- The damped part of the solution vanishes exponentially after relatively small time intervals.
- Periodic attractor to which the motion eventually converges.
- Amplitude and frequency responses.

We seek an approximate solution of Eqn. (5) as an asymptotic series in powers of ϵ of the following form:

$$x(t) = x_0(t) + \epsilon\, x_1(t) + \epsilon^2\, x_2(t) + \dots$$

Analytical results

The Fourier series expansion of the periodic solution $\hat{x}(t)$:

$$\hat{x}(t) = \sum_{k=0}^{\infty} \epsilon^k B_k \exp\{(2k+1)i\omega t\}, \tag{7}$$

whose coefficients are recursively given by the expression:

$$B_k = \frac{-1}{\Omega_1^2 - [(2k+1)\omega]^2} \left(B^3_{\frac{k-1}{3}} \delta_{k,3\upsilon} + 3 \sum_{\substack{i+2j=k-1 \\ i>j}} B_i B_j^2 + 3 \sum_{\substack{2i+j=k-1 \\ i>j}} B_i^2 B_j + 6 \sum_{\substack{i+j+l=k-1 \\ i>j}} B_i B_j B_l \right), \tag{8}$$

for $k \geq 1$, with $B_0 = \dfrac{F}{\Omega_1^2 - \omega^2}$ and $\delta_{n,m}$=1 for $n = m$ and 0 for $n \neq m$.

Numerical results I

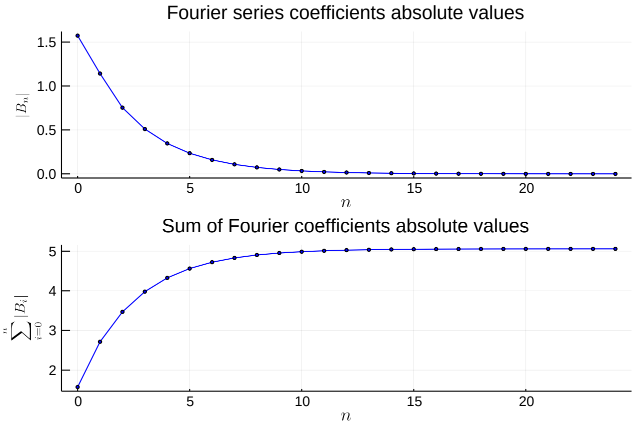

Figure 1: Illustration of the (absolute) convergence of the Fourier series expansion of the periodic solution for the nonlinear problem. Parameters used: $(\mu, f, g, \omega, \epsilon) = (0.05, 0.8, 0.1, 0.7, 0.1)$.

Numerical results II

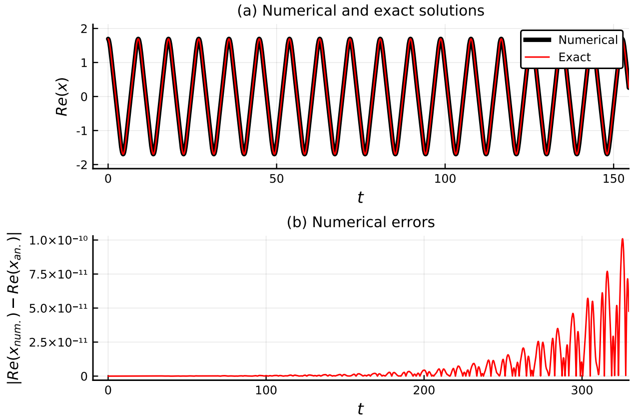

Figure 2: Top: Numerical (black) and analytical (red) trajectory of the nonlinear system of Eqn. (5) for $\epsilon = 0.1$. Bottom: Time plot of the error, calculated as the distance between the numerical and the analytical solution, i.e. $|\mathrm{Re}(x_{\mathrm{an}}) - \mathrm{Re}(x_{\mathrm{num}})|$.

Numerical results III

- Potential function has no saddle points $\rightarrow$ all motion is bounded.
- Numerical origin of divergences: the time t_d where the solutions begin to diverge depends on the selected computational precision.

We set $(k, h, g, \epsilon) = (1., 0.1, 0.8, 0, 0.05)$ and vary the forcing frequency ω and the forcing amplitude f (Figs. 3-4).

> The variation of the driving frequency/amplitude results in a great increase of complexity in the morphology of the periodic solutions.

Forcing frequency variation

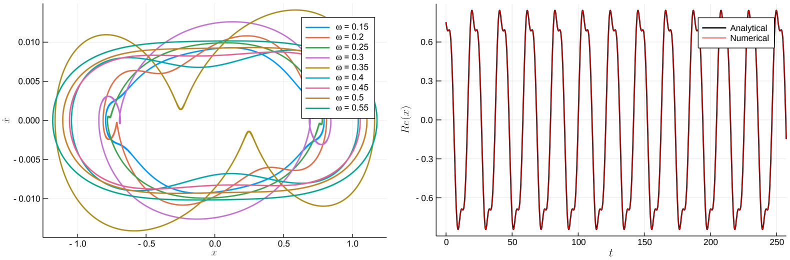

Figure 3: (a) Phase space projections of the real parts of the displacement x and the velocity $\dot{x}$. (b) Time plots of the real parts of the analytical (black) and numerical (red) solutions with parameters as in (a) and $\omega = 0.3$.

Forcing amplitude variation

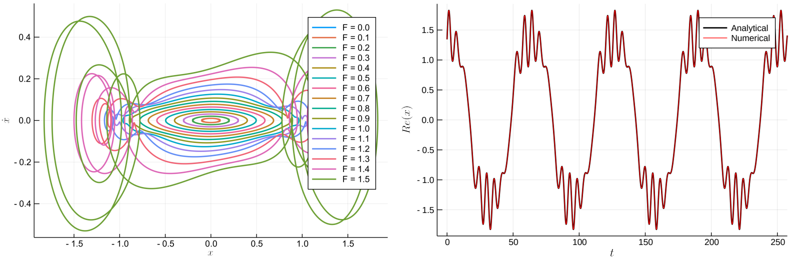

Figure 4: (a) Phase space projections of the real parts of the displacement x and the velocity $\dot{x}$. (b) Time plots of the real parts of the analytical (black) and numerical (red) solutions with parameters as in (a) and $F = 0.3$.

Response curves

- Nonlinearity of the equation of motion → more frequencies are present in the solution.
- Amplitude response curve: ratio of the amplitude of the nonlinear attractor to the amplitude of the driving force, with respect to the frequency ratio ω/ω_1.
- Frequency response curve: phase delay angle of the forced oscillation as a function of ω/ω_1.

Amplitude response

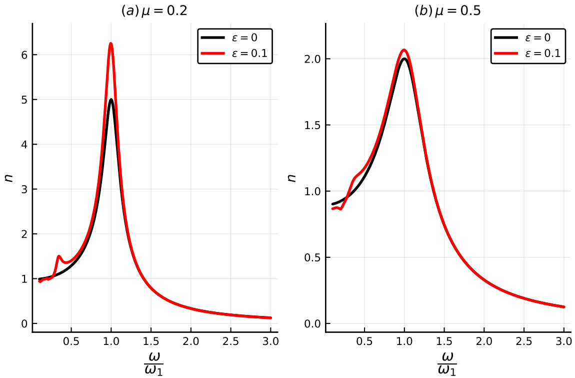

Figure 5: Magnification factor n (amplitude response) with respect to the frequency ratio ω/ω_1 for the system with cubic nonlinearity.

Phase response

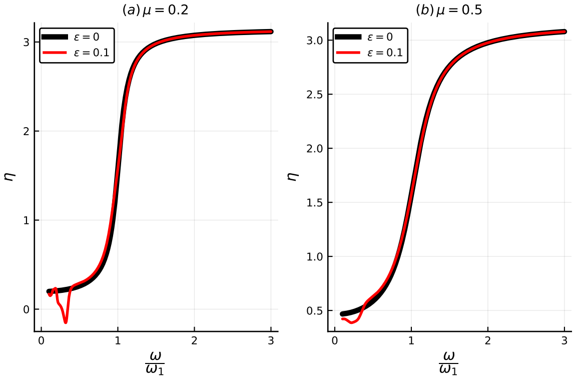

Figure 6: Phase response with respect to the frequency ratio ω/ω_1 for the system with cubic nonlinearity ($\epsilon = 0.1$), superimposed with the associated response of the linear system ($\epsilon = 0$).

SDOF Reid model

The model

$$M\ddot{x} + c\left|\frac{x}{\dot{x}}\right|\dot{x} + kx + \epsilon x^3 = f \sin \omega t.$$

- The original model is strictly speaking nonlinear, due to the sign–function term, but this has limited implications for the dynamical behavior of the system ("quasi–linear").
- Real solutions, no numerical instabilities.
- Amplitude and frequency responses: Although for high forcing frequencies the two systems behave almost indistinguishably, for low frequencies the model of Eqn. (6) exhibits secondary resonances.
- Nonlinearity: Multiple periodic solutions.

Amplitude response curves

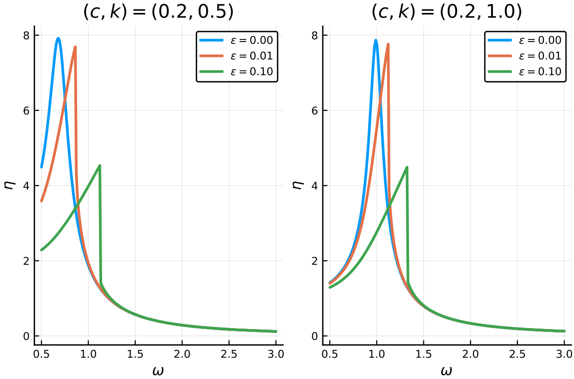

Figure 7: Amplitude response curves of Reid's model for varying $\epsilon \in \{0, 0.01, 0.1\}$. We set the damping coefficient to $c = 0.2$ and use two different values for the linear stiffness, namely $k \in \{0.5, 1\}$.

Nonlinear stiffness effects

- The peaks of the curves in Fig. 7 are influenced by the nonlinearity, as higher values of ϵ lead to peaks at higher values of ω.
- The increase of the stiffness parameter results in decrease of the magnification factor.
- High values of damping $\rightarrow$ unique stable periodic solution.
- Low values of damping $\rightarrow$ emergence of stable periodic orbits with period different than T^* (forcing period).
- Complex basin of attraction structure.

Numerical results

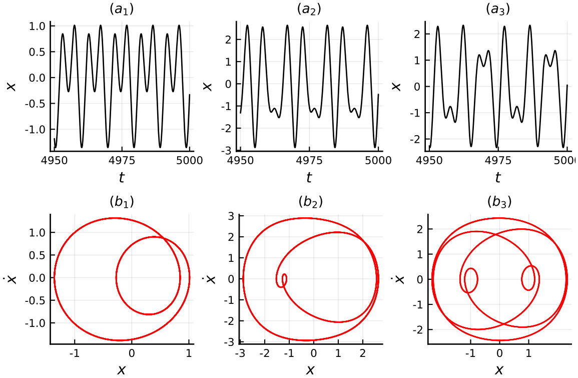

Figure 8: Time $(t, x(t))$ and phase $(x, \dot{x})$ plots of periodic solutions for the modified Reid's model, with parameters $(c, k, f, \omega, \epsilon) = (0.01, 0.3, 1.1, 1.3, 0.1)$. The associated periods are $2T^*, 3T^*, 5T^*$ for the first, second and third column, respectively.

Basins of attraction

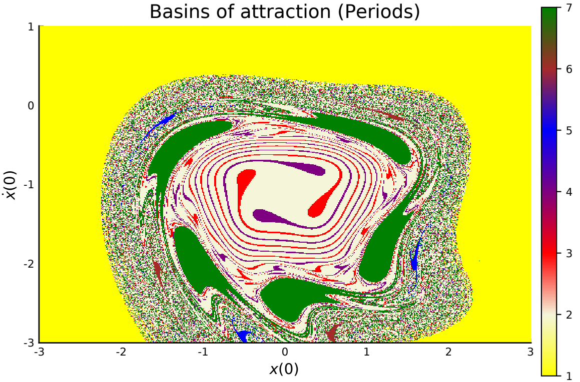

Figure 9: Basins of attraction of the modified Reid's model for parameters $(c, k, f, \omega, \epsilon) = (0.01, 0.3, 1.1, 1.3, 0.1)$. We have used the coding 1 and 2 for orbits with period $T = T^*$, 3 and 4 for $T = 2T^*$, 5 and 6 for $T = 3T^*$ and 7 for the $T = 5T^*$.

Arrays of coupled nonlinear Reid oscillators

The model

- Coupled nonlinear Reid oscillators: collective dynamical behavior.
- Desirable collective dynamics → engineering applications.
- Nonlinear supratransmission: Excitation of nonlinear modes & energy transfer.

Equations of motion for N–DOF system

For $j = 1, \ldots, N$:

$$M\ddot{x}_j = -c\left|x_j\right|\tanh\{\tau\dot{x}_j\} - k\left(-x_{j-1} + 2x_j - x_{j+1}\right) - \epsilon\left(-\left(x_{j+1} - x_j\right)^3 + \left(x_j - x_{j-1}\right)^3\right), \tag{9}$$

subjected to the boundary values at the origin and the end:

$$x_0(t) = f\sin\omega t \quad \text{and } x_{N+1}(t) = 0, \quad t \in \mathcal{T} \subseteq \mathbb{R}+ .$$

4 dof system I

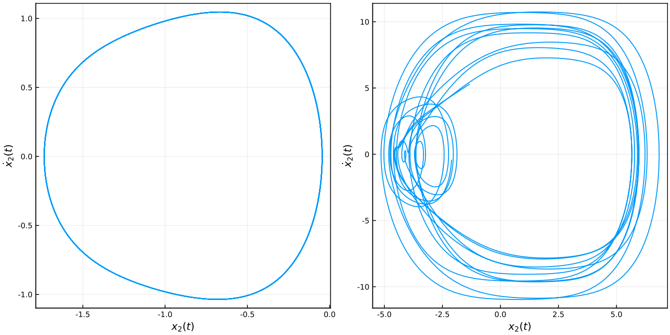

Figure 10: Phase plots of the second oscillator of a 4 dof system, using different (random) initial conditions. Notice that for different initial conditions we can observe either a periodic or a quasi-periodic motion. The parameters used were $(c, k, f, \omega, \epsilon) = (0.01, 0.3, 1.1, 1.3, 0.1)$.

4 dof system II

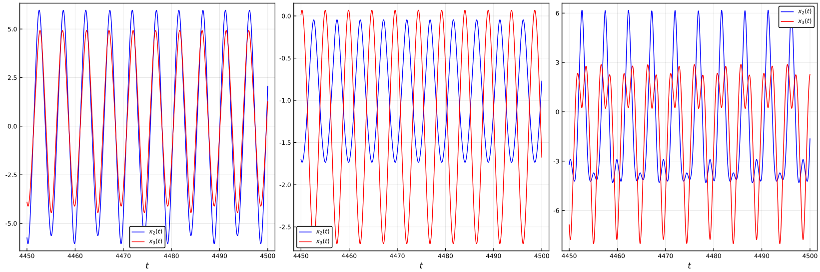

Figure 11: Trace plots of the second (blue) and the third (red) particle displacements, using three different combinations of (random) initial conditions. The parameters used were $(c, k, f, \omega, \epsilon) = (0.01, 0.3, 1.1, 1.3, 0.1)$.

20 dof system

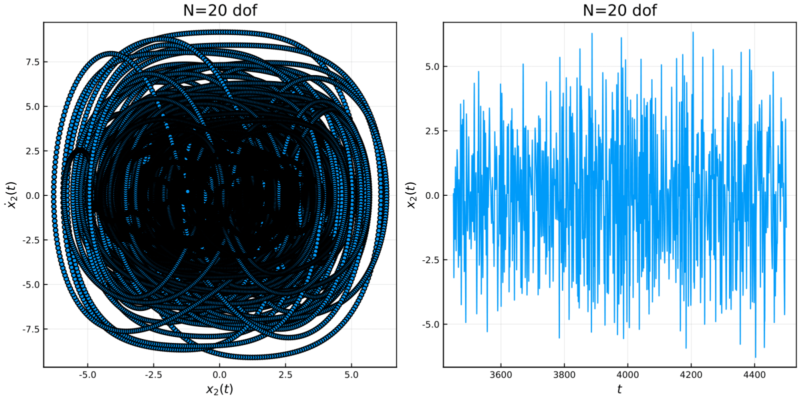

Figure 12: Phase (left) and time (right) plots of the second particle of a system with 20 dofs, exhibiting chaotic motion. The parameters used were $(c, k, f, \omega, \epsilon) = (0.01, 0.3, 1.1, 1.3, 0.1)$.

Energy transfer

- Rich dynamical behavior.
- Initiate the medium at rest, namely

$$x_j(0) = \dot{x}_j(0) = 0,\ \forall j \in \{1, \ldots, N\}$$

  and gradually increase the driving amplitude of the first ("driving") oscillator.
- Is there a critical forcing amplitude (f_{cr}) regarding the energy transfer?
- Sudden transmission of energy above a sharp threshold amplitude of periodic boundary excitations.
- Avoid the forbidden band gap: $\omega > 2$.

Numerical criterion

In order to obtain the bifurcation plots in the (ω, f)–parameter space, we developed a numerical criterion in order to "automatically" identify the occurrence of supratransmission.

$$\mathcal{D}_f = \frac{1}{n_T} \sum_{i=1}^{N} \sum_{j=1}^{n_T} x_i^2(t_j),$$

Critical amplitude f_{cr}: the *first* amplitude resulting in $\Delta\mathcal{D}_f$ exceeding a certain threshold Δ_{th} , that is for a sequence of driving amplitudes $f_1, f_2, \ldots, f_k$ we have that:

$$f_{cr} : cr = \arg \min_{1 \leq i \leq k} \left\{ \mathcal{D}_{f_i} - \mathcal{D}_{f_{i-1}} > \Delta_{th} \right\}.$$

Supratransmission I

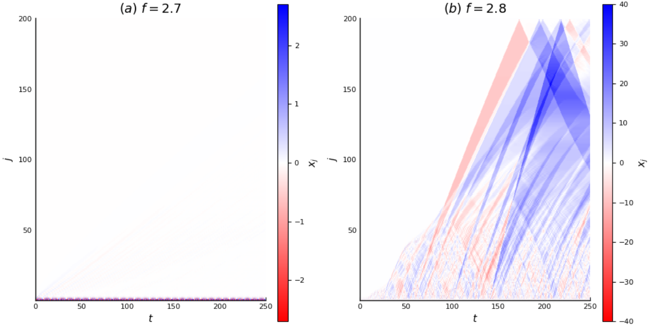

Figure 13: Colormaps of the displacement solutions of Eqs. (9) for parameter values $(c, k, \omega, \epsilon) = (0.01, 0.3, 2.5, 0.1)$. (a) $f = 2.7$ and (b) $f = 2.8$.

Supratransmission II

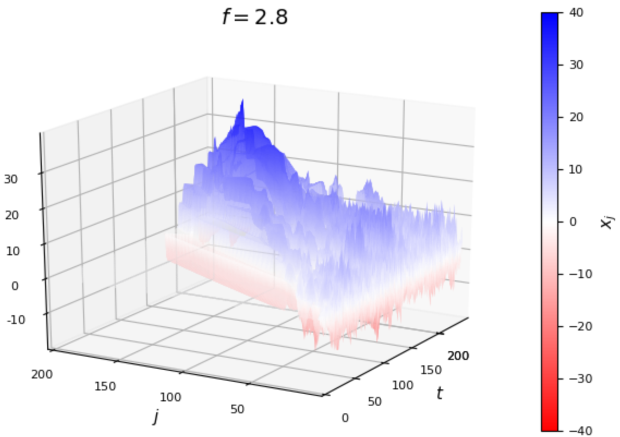

Figure 14: Graphs of the displacement solutions of Eqs. (9) for parameter values $(c, k, \omega, \epsilon) = (0.01, 0.3, 2.5, 0.1)$ and $f = 2.8$

Effect of the damping terms

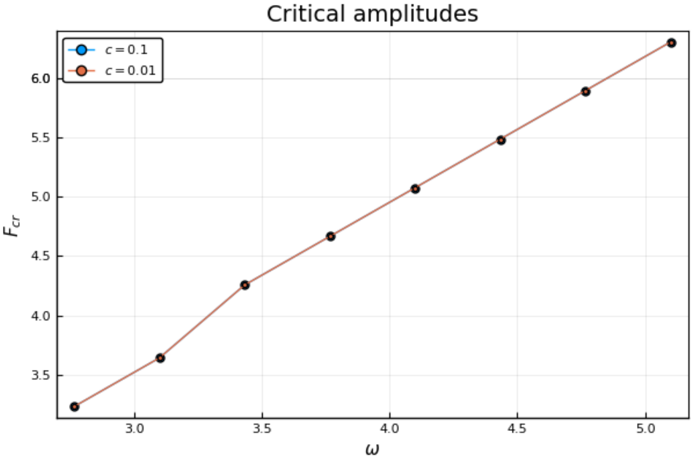

Figure 15: Critical amplitudes with respect to the forcing frequencies, with $(k, \epsilon) = (0.3, 0.1)$, for damping parameter $c \in \{0.01, 0.1\}$.

Effect of the nonlinear terms

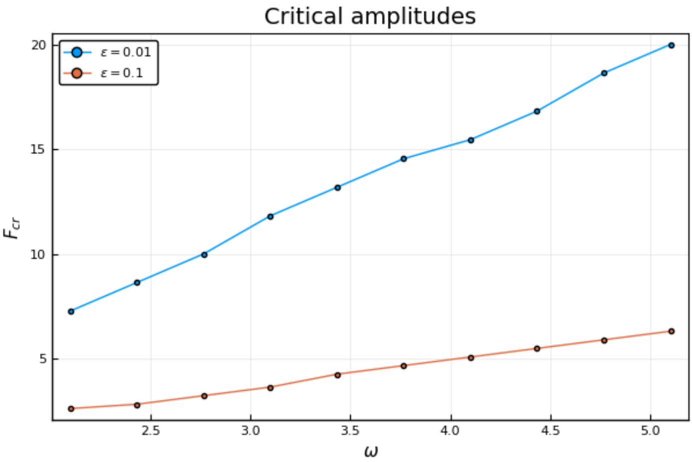

Figure 16: Critical amplitudes with respect to the forcing frequencies, with $(k, c) = (0.3, 0.01)$, for nonlinearity parameter $\epsilon \in \{0.01, 0.1\}$.

Effect of the coupling terms

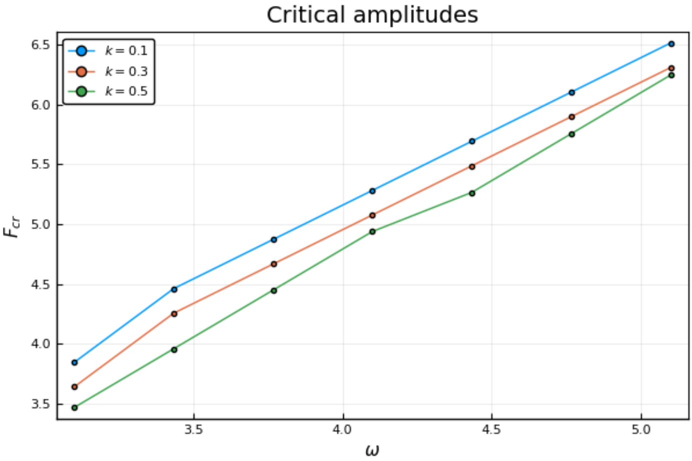

Figure 17: Critical amplitudes with respect to the forcing frequencies, with $(c, \epsilon) = (0.1, 0.1)$, for coupling strength $k \in \{0.1, 0.3, 0.5\}$.

Comments

- The values of the damping parameter do not affect the values of f_{cr}, as they are not taken into account in the coupling terms. Moreover, it is interesting that the critical amplitudes are approximately linearly increasing with respect to the $\omega \in (2.5, 5.5)$.
- Higher values of ϵ correspond to lower values of f_{cr} (not affecting the linear increase wrt ω). This means that when the couplings are stronger, it is "easier" to excite the nonlinear modes, in the sense that the critical amplitudes are lower.
- Higher values of k correspond to lower values of f_{cr} (not affecting the linear increase wrt ω). When the nonlinearities are stronger, it is "easier" to excite the nonlinear modes, in the sense that the critical amplitudes are lower.

Random periodic forcing I

Effect of "random periodic forcing": We perturb only the first particle (i.e. the one that is periodically driven). Formally, we have (same as above) for $j = 1, \ldots, N$:

$$M\ddot{x}_j = -c\left|x_j\right|\tanh\{\tau\dot{x}_j\} - k\left(-x_{j-1} + 2x_j - x_{j+1}\right) - \epsilon\left(-\left(x_{j+1} - x_j\right)^3 + \left(x_j - x_{j-1}\right)^3\right), \tag{10}$$

subjected to the (random) boundary values at the origin and the end:

$$x_0(t) = f\sin\omega t + \sigma\,\xi(t) \quad \text{and } x_{N+1}(t) = 0, \quad t \in \mathcal{T} \subseteq \mathbb{R}+,$$

where σ denotes the noise intensity and $\xi(t)$ is additive white noise.

Random periodic forcing II

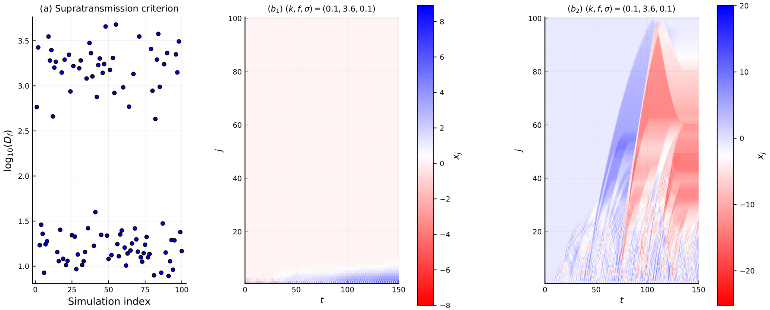

Figure 18: (a) Semilogarithmic plots of 100 simulations of the stochastic system. We present the values of (the numerical criterion index) $\log_{10}\left(\mathcal{D}_f\right)$, for array size $N = 100$. $(b_1) - (b_2)$ Colormaps of the displacement solutions for 2 different realizations of the stochastic system of (a). The other parameters are set to $(c, \omega, \epsilon) = (0.1, 3, 0.1)$.

Supratransmission probability I

- Effects of the forcing amplitude and noise intensity on the supratransmission probability.
- Higher values of either f or σ (or lower values of the coupling strength) generally result in higher probabilities.
- Heatmaps of the supratransmission probability taking into account *both* f and σ, for varying array sizes $N \in \{100, 200\}$.
- For low values of noise intensity, the system behaves more "deterministically", meaning that it has a "0–1" like behavior.
- The perturbed system can excite the nonlinear modes more "easily", namely at lower amplitudes wrt to associated unperturbed system.

Supratransmission probability II

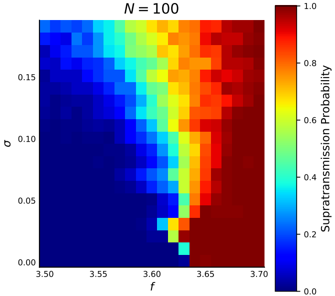

Figure 19: Colormaps of the supratransmission emergence probability with respect to the forcing amplitude and the noise intensity for varying array sizes $N \in \{100, 200\}$. The other parameters are set to $(c, k, \omega, \epsilon) = (0.1, 0.1, 3, 0.1)$. The critical amplitude of the associated unperturbed system is slightly above 3.7.

Different approach: Distribution of f_{cr}

- Complete given set of parameters.
- We gradually increase the forcing amplitude, keeping the same noise realization.

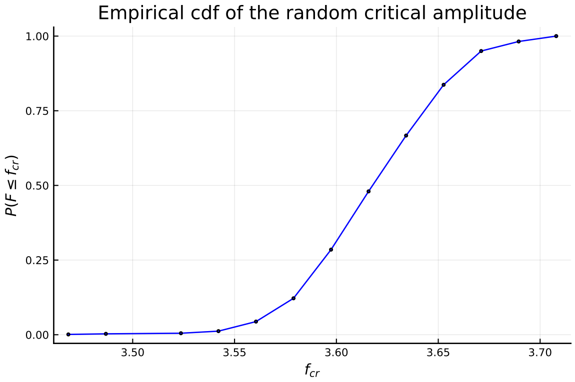

Figure 20: Empirical cdf of the obtained critical amplitudes.

Conclusions & Future Research

Conclusions

- The nonlinear extension of the Bishop's hysteretic damping model suffers (as the original one) from spurious numerical instabilities.
- The nonlinear extension of Reid's model is free from such errors and has a rich dynamical behavior, with different stable periodic solutions in the SDOF case and complex basins of attraction.
- Arrays of coupled nonlinear Reid oscillators exhibit the nonlinear supratransmission phenomenon, which is robust under random periodic forcing.

Future Work

Natural direction of future research include:

- Dynamical behavior under different forms of random periodic forcing.
- Statistical properties of the coupled oscillators.
- Relation of the supratransmission phenomenon with the (perturbed) soliton solution of the modified KdV PDE: $u_t + u_{xxx} + au^2 u_x = 0$.

References I

Tassos Bountis, Konstantinos Kaloudis, Christos Spitas (2020)
Periodically Forced Nonlinear Oscillators With Hysteretic Damping
Journal of Computational and Nonlinear Dynamics

Tassos Bountis, Konstantinos Kaloudis, Christos Spitas (2020)
Supratransmission phenomena in a one-dimensional array of coupled nonlinear Reid oscillators.
In preparation

Bishop, R.E.D. (1955)
The treatment of damping forces in vibration theory.
The Aeronautical Journal

Reid, T.J. (1956)
Free vibration and hysteretic damping.
The Aeronautical Journal

References II

Pace S., Reiss K.A., David K. Campbell D.K. (2019)
The β–Fermi-Pasta-Ulam-Tsingou recurrence problem.
Chaos

Geniet F. and Leon J. (2002)
Energy transmission in the forbidden band gap of a nonlinear chain.
PRL

Thank you!